J. Fluid Mech. (1993), *vol.* 246, *pp.* 593–612

Water entry of two-dimensional bodies

By R. ZHAO[1] AND O. FALTINSEN[2]

[1] Marintek A/S, PO Box 4125 Valentinlyst, Trondheim, Norway

[2] Division of Marine Hydrodynamics, Norwegian Institute of Technology, Trondheim, Norway

(Received 13 January 1992 and in revised form 4 August 1992)

A numerical method for studying water entry of a two-dimensional body of arbitrary cross-section is presented. It is a nonlinear boundary element method with a jet flow approximation. The method has been verified by comparisons with new similarity solution results for wedges with deadrise angles varying from 4° to 81°. A simple asymptotic solution for small deadrise angles α based on Wagner (1932) agrees with the similarity solution for small α.

1. Introduction

Impulse, or slamming, loads with high pressure occur during impact between a blunt body and the water. The study presented in this paper has most relevance to slamming loads on ship hulls, but the findings are also important for studying slamming on the underside of the deck between the hulls of multihull vessels.

Slamming has been extensively studied by Wagner (1932), Garabedian (1953), and Mackie (1969). Armand & Cointe (1986), Cointe (1991) and Howison, Ockendon & Wilson (1991) have further developed and extended Wagner's theory by using matched asymptotic expansions for impacting bodies with small deadrise angles. Dobrovol'skaya (1969) presented similarity solutions for wedges that are forced with a constant velocity through the free surface. The solution is applicable for any deadrise angle α, but the solution is not available in explicit form and numerical results were only presented for $\alpha \geqslant 30°$. Fraenkel (1991, and personal communication) has proved existence and uniqueness for the similarity solution of Dobrovol'skaya for all α. Finally Korokbin & Pukhnochov (1988) have given an excellent review on slamming.

The paper presents a numerical method for studying water entry of a two-dimensional body of arbitrary cross-section. The water is assumed incompressible and the flow irrotational. This means that the impact velocity is not so high that compressibility effects in the water matter. In practice this is not a severe limitation. It is assumed that no air pocket is created during impact. This means that α has to be larger than 2–3°. The exact nonlinear free-surface conditions without gravity are satisfied. Important features of the solution method are how the jet flow occurring at the intersection between the free surface and the body is handled, and how conservation of fluid mass is satisfied in areas of high curvature of the free surface. The method checks that conservation of mass, momentum and energy are satisfied.

Greenhow (1987) has studied a similar problem by using Vinje & Brevig's (1980) nonlinear numerical method. The agreement with the similarity solution was satisfactory for $\alpha > 60°$, but poor for $\alpha = 45°$ owing to difficulties in following the jet flow.

The authors are not aware of numerical similarity solution results for wedges with

deadrise angles lower than 30°, which is probably due to numerical difficulties in solving the integral equations. As a part of the verification process of our numerical method it was decided to derive numerical similarity solution results for wedges with α from 4° to 81°. The method was based on the analytical formulation by Dobrovol'skaya (1969), but a different numerical solution technique was used in order to handle smaller deadrise angles accurately. These calculations require modern computing facilities. The similarity solution results have been verified by convergence tests and by checking that the free-surface conditions, the body boundary condition, the far-field representation, conservation of mass, momentum and energy are all satisfied.

At small deadrise angles it is possible to use Wagner's (1932) local jet flow analysis in combination with matched asymptotic expansions. A simple formula for the slamming pressure on wedges has been derived and shown to give good agreement with both the similarity solution and our numerical method for small deadrise angles.

2. Theory

Consider a two-dimensional body that is forced vertically through the initially calm free surface of an unbounded ocean. No air pocket between body and free surfaces is assumed to be created during the impact. The origin of the coordinate system is in the plane of the undisturbed water surface. The z-axis is positive upwards and is a symmetry line for the cross-section. The y-axis is in the undisturbed water plane.

The fluid is assumed to be incompressible and the flow irrotational so that there exists a velocity potential ϕ that satisfies the Laplace equation

$$\frac{\partial^2\phi}{\partial y^2}+\frac{\partial^2\phi}{\partial z^2}=0 \tag{2.1}$$

in the fluid domain. The pressure is set equal to a constant atmospheric pressure on the free surface. The effect of gravity is neglected compared with the large fluid accelerations. (However including gravity would cause no difficulties.) The kinematic free-surface condition is that a fluid particle remains on the free surface. Hence the motion of the free surface may be found by integrating the fluid velocity. The dynamic free-surface condition (applied on the exact free surface) can be written as

$$\frac{\mathrm{D}\phi}{\mathrm{D}t}=\frac{1}{2}\left[\left(\frac{\partial\phi}{\partial y}\right)^2+\left(\frac{\partial\phi}{\partial z}\right)^2\right], \tag{2.2}$$

where $\mathrm{D}/\mathrm{D}t$ means the substantial derivative and t is the time variable. The body boundary condition on the wetted body surface is written as

$$\frac{\partial\phi}{\partial n}=-Vn_3 \tag{2.3}$$

where $\boldsymbol{n}=(n_2,n_3)$ is the unit normal vector to the body surface and $\partial/\partial n$ is the derivative along this normal vector. The positive direction of $\boldsymbol{n}$ is into the fluid domain. V is the body velocity along the negative z-axis.

It is assumed that a jet flow is created at the intersection between the free surface and the body surface. The pressure is set equal to atmospheric pressure in the upper part of the jet. We simplify the solution by defining an instantaneous fluid domain

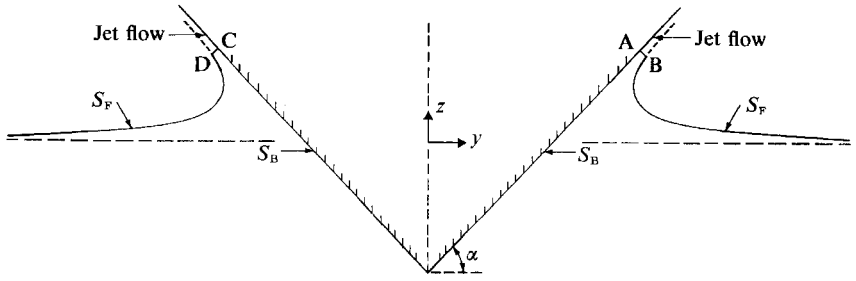

FIGURE 1. Definitions of coordinate system and control surfaces used in the numerical solution of water entry of a wedge; α = deadrise angle.

Ω that does not contain the whole jet flow. The velocity potential ϕ for the flow inside the fluid domain is represented by Green's second identity, i.e.

$$2\pi\phi(y,z) = \int_S \left[\frac{\partial\phi(\eta,\zeta)}{\partial n(\eta,\zeta)}\log r - \phi(\eta,\zeta)\frac{\partial \log r}{\partial n(\eta,\zeta)}\right] ds(\eta,\zeta), \tag{2.4}$$

where $r = [(y-\eta)^2+(z-\zeta)^2]^{\frac{1}{2}}$. The surface S enclosing Ω consists of AB, CD, S_B, S_F and S_∞, where S_∞ is a control surface far away from the body. AB is shown in figure 1. The angle between the body surface and AB is 90°, while the angle between AB and the free surface is close to 90°. The line AB is in an area where the jet starts and where the pressure can be approximated by atmospheric pressure (see later). CD is symmetric with AB about the z-axis. S_B is the wetted body surface between points A and C. S_F is the free surface outside points B and D and inside S_∞. S_∞ is chosen so far away that its contribution in (2.4) is zero. The contribution from the free-surface integral can be rewritten. For $|y| > b(t)$, where $b(t)$ is a large number dependent on time t, the flow can be represented by a vertical dipole in infinite fluid, i.e.

$$\phi(y,z) \sim \frac{A(t)\,z}{z^2+y^2}. \tag{2.5}$$

By setting $\zeta = 0$ the integral from $-\infty$ to $-b$ and from b to ∞ of (2.4) can be written as

$$-A(t)\left\{\frac{\log[(b\pm y)^2+z^2]^{\frac{1}{2}}}{b} \pm \frac{y}{y^2+z^2}\log\frac{[(b\pm y)^2+z^2]^{\frac{1}{2}}}{b} + \frac{z}{y^2+z^2}\left[\operatorname{sgn}(z)\tfrac{1}{2}\pi - \arctan\left(\frac{b\pm y}{z}\right)\right]\right\}, \tag{2.6}$$

where the plus sign is valid for the integral from $-\infty$ to $-b$ and the minus sign for the integral from b to ∞.

The problem is solved as an initial value problem where the velocity potential and the free-surface elevation are set equal to zero at the initial time. By using the kinematic and dynamic free-surface conditions, one can follow how the free surface S_F moves and how the velocity potential changes on the free surface. In the initial phase of the flow, AB and CD are not used. When AB and CD are introduced, their motions are found by assuming a one-dimensional flow there and integrating the fluid velocity. This implies that the deadrise angle cannot be too large. Since the pressure

is assumed to be atmospheric at AB and CD, and AB and CD follow the fluid motion, (2.2) can be used to determine the change in ϕ on AB and CD.

At each time instant one solves an integral equation resulting from (2.4) by letting (y, z) be points on S_B, AB, CD and S_F inside $|y| < b(t)$. On AB, CD and S_F inside $|y| < b(t)$, the velocity potential is known and the normal velocity $\partial\phi/\partial n$ is unknown, while on S_B ϕ is unknown and $\partial\phi/\partial n$ is known. The unknown $A(t)$ in (2.5) is found by requiring continuity in the velocity potential at $|y| = b(t)$. The pressure on the body follows from Bernoulli's equation.

In the numerical evaluation of (2.4), the free surface S_F inside $|y| = b(t)$, and body surface S_B, are divided into a number of straight line segments, on which ϕ and $\partial\phi/\partial n$ are set constant. In areas of high curvature on S_F and S_B, as well as close to the jet area on S_B, a high density of segments is necessary. One segment is used to represent AB and CD. Following the assumption of one-dimensional flow, and in view of the body boundary condition, $\partial\phi/\partial n$ is constant and ϕ has a linear variation over AB and CD. In the initial phase of the flow AB and CD are not used; instead S_F is assumed to intersect S_B. Owing to confluence of boundary conditions at the intersection, it is important numerically that fluid variables are not evaluated at the intersection point.

When S_F becomes nearly parallel to S_B, AB and CD are introduced, but we cannot know exactly *a priori* at what angle between S_F and S_B this should occur. From the similarity solution for wedges we know that it should be small if α is not too large. In results with $\alpha \leqslant 60°$ we have introduced AB and CD when the angle between S_F and S_B is $\frac{1}{30}\pi$ at the intersection. When $\alpha = 81°$, we have used $\frac{1}{15}\pi$ as a limiting angle. As long as the limiting angle is small, its choice will not in general influence the flow and the pressure distribution. An exception is the shape of the pressure distribution on the body in a small neighbourhood of AB and CD. AB and CD are introduced by constructing a normal to the body surface from the second end point of the first segment on S_F on each side of the body. The first segment on S_F is the one starting from the intersection between the body and the free surface. The linear variation of ϕ over AB and CD is obtained by using the body boundary condition and interpolations of the potentials at the midpoints of the first and second segments on S_F on each side of the body.

After AB and CD are introduced, they follow the fluid motion by using the velocities normal to AB and CD at their midpoints. The linear variations of ϕ over AB and CD are found by using (2.2) at the midpoints of AB and CD, and by using the body boundary conditions at A and C. During the time integration, the relative angles between the body surface and the second segment on S_F from respectively B and D are monitored. If this angle is smaller than the limiting angle, new segments AB and CD introduced by excluding the first segments on S_F relative to B and D. The velocity potential on the midpoints of AB and CD are obtained by linear interpolation.

The integral equation is satisfied at the midpoint of each segment. In the time integration of the free-surface position, it is important to satisfy conservation of fluid mass carefully. This means that the rate of change with time of the water volume above $z = 0$ should be equal to the rate of change with time of the body displacement below $z = 0$.

The time integration of the free surface can be explained using figure 2. $P(j, i)$ are endpoints of segments at time instant i. Based on the points $P(j+2, i)$, $P(j+1, i)$ and $P(j, i)$, one obtains a first estimate of $P(j+\frac{1}{2}, i)$ by fitting a curve of constant

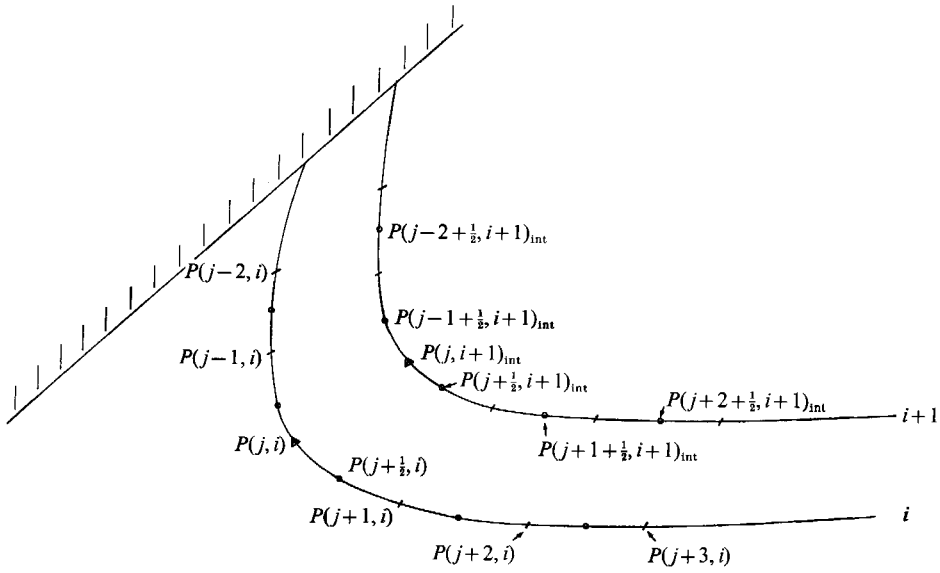

FIGURE 2. Definitions of points used in the description and motion of the free surface by the nonlinear boundary element method described in §2.

curvature through the points, and letting $P(j+\frac{1}{2}, i)$ be situated at the midpoint along the curve between $P(j, i)$ and $P(j+1, i)$. A second estimate of $P(j+\frac{1}{2}, i)$ is obtained similarly but with the points, $P(j+1, i)$, $P(j, i)$ and $P(j-1, i)$. The final value of $P(j+\frac{1}{2}, i)$ is the average of the first and second estimate of $P(j+\frac{1}{2}, i)$. The fluid velocity at $P(j+\frac{1}{2}, i)$ is set equal to the numerical value of the velocity at the midpoint of the straight line segment between $P(j, i)$ and $P(j+1, i)$. It is $P(j+\frac{1}{2}, i)$ that is followed in time and not the midpoint of the straight line segment. This avoids large errors in conservation of fluid mass. Close to AB, CD and $|y| = b(t)$ this procedure is unnecessary since the curvature of the free surface is low. The time stepping of $P(j+\frac{1}{2}, i)$ is done in two steps. First an intermediate new position $P(j+\frac{1}{2}, i+1)_{\text{int}}$ at time instant $i+1$ is found, based on the velocity V calculated at the midpoint of the straight line segment between $P(j, i)$ and $P(j+1, i)$. The change in the position between $P(j+\frac{1}{2}, i+1)_{\text{int}}$ and $P(j+\frac{1}{2}, i)$ is $V\Delta t$, where Δt is the time difference between time instants $i+1$ and i. The change in the velocity potential is found similarly. Based on the points $P(j-\frac{3}{2}, i+1)_{\text{int}}$, $P(j-\frac{1}{2}, i+1)_{\text{int}}$, $P(j+\frac{1}{2}, i+1)_{\text{int}}$ and $P(j+\frac{3}{2}, i+1)_{\text{int}}$ one calculates $P(j, i+1)_{\text{int}}$ by fitting two curves of constant curvature through the points, and finding $P(j, i+1)_{\text{int}}$ in the same way as described earlier for $P(j+\frac{1}{2}, i)$. Between $P(j-1, i+1)_{\text{int}}$ and $P(j, i+1)_{\text{int}}$ straight line segments are formed. Velocities are found by solving the boundary value problem with the intermediate positions of the free surface. By interpolation one finds the velocity at $P(j+\frac{1}{2}, i+1)_{\text{int}}$. The average velocity V_{av} at $P(j+\frac{1}{2}, i+1)_{\text{int}}$ and $P(j+\frac{1}{2}, i)$ is used to find $P(j+\frac{1}{2}, i+1)$. The change in position between $P(j+\frac{1}{2}, i+1)$ and $P(j+\frac{1}{2}, i)$ is $V_{\text{av}}\Delta t$. V_{av} is also used in (2.2) to find the change in the velocity potential for the fluid point $j+\frac{1}{2}$ on the free surface. The further steps to find the free-surface segments are similar to those for the intermediate position.

The pressure p on the body is calculated by means of Bernoulli's equation. The

$\partial\phi/\partial t$-term is found by generalizing the concept of substantial derivative. One introduces

$$\frac{\mathrm{D}'\phi}{\mathrm{D}'t} \equiv \frac{\partial\phi}{\partial t} + \boldsymbol{U}\cdot\nabla\phi, \tag{2.7}$$

where $\mathrm{D}'\phi/\mathrm{D}'t$ is the change in ϕ when one follows a point that moves with velocity $\boldsymbol{U}$. $\boldsymbol{U}$ does not need to be the fluid velocity. $\mathrm{D}'\phi/\mathrm{D}'t$ for the midpoint of segment j at time $t+\frac{1}{2}\Delta t$ is approximated by $\Delta\phi/\Delta t$, where $\Delta\phi$ is the change in the velocity potential on segment j from t to $t+\Delta t$. The velocity $\boldsymbol{U}$ in (2.7) is the velocity of the midpoint of segment j, estimated at $t+\frac{1}{2}\Delta t$ by the positions of segment j at t and $t+\Delta t$. The fluid velocity $\nabla\phi$ at time $t+\frac{1}{2}\Delta t$ at segment j is found by averaging the values at t and $t+\Delta t$. This is used in both (2.7) and the quadratic velocity term in Bernoulli's equation.

The convergence of the numerical procedure has been tested by changing the number of body and free-surface segments, the time step and the value of $b(t)$. Conservation of mass, momentum and energy are also checked. Conservation of mass has been discussed earlier. In checking conservation of momentum the following equation can be used:

$$-\int_{S_B}(p-p_0)\,n_3\,\mathrm{d}s = \frac{\mathrm{d}}{\mathrm{d}t}\left[\int_S \rho\phi n_3\,\mathrm{d}s\right]. \tag{2.8}$$

Here p_0 is the atmospheric pressure and ρ is the mass density of the water. Equation (2.8) can be shown by using expressions given by Faltinsen (1977) by neglecting the effect of gravity and generalizing the derivation by including the effect of AB and CD. As long as AB and CD move with the fluid velocity, (2.8) is correct.

The left-hand side of (2.8) is calculated directly from Bernoulli's equation. The right-hand side can also be written as

$$\int_S \rho\frac{\partial\phi}{\partial t}n_3\,\mathrm{d}s + \rho\int_S \frac{\partial\phi}{\partial z}U_n\,\mathrm{d}s, \tag{2.9}$$

where U_n is the normal velocity of the surface S (see Newman 1977, p. 133).

The energy $E(t)$ in the fluid domain Ω consists only of kinetic energy. It can be written as

$$E(t) = \rho\,0.5\int\!\!\int_\Omega \nabla\phi\cdot\nabla\phi\,\mathrm{d}\tau = -\rho\,0.5\int_S \phi\frac{\partial\phi}{\partial n}\mathrm{d}s. \tag{2.10}$$

The fluid domain Ω is defined in connection with (2.4). From (2.10) $\mathrm{d}E(t)/\mathrm{d}t$ is calculated. This is equal to the rate of work $\mathrm{d}w/\mathrm{d}t$ done on the body where

$$\frac{\mathrm{d}w}{\mathrm{d}t} = -\int_S (p-p_0)\,n_3\,\mathrm{d}s\,V(t). \tag{2.11}$$

Figure 3 gives an example on how well conservation of mass, momentum and energy is satisfied for a wedge with $\alpha = 20°$ that is forced with constant velocity through the free surface. The figure also shows maximum pressure $p_{\max}$ on the body surface and the z-coordinate $z_{\max}$ of $p_{\max}$ as a function of non-dimensional time t/T_1, where $t = T_1$ corresponds to the instant when AB and CD are first introduced. The figure also shows the development of ratios between alternative calculations of mass, energy and force. The mass ratio is the ratio between the time derivative of the fluid

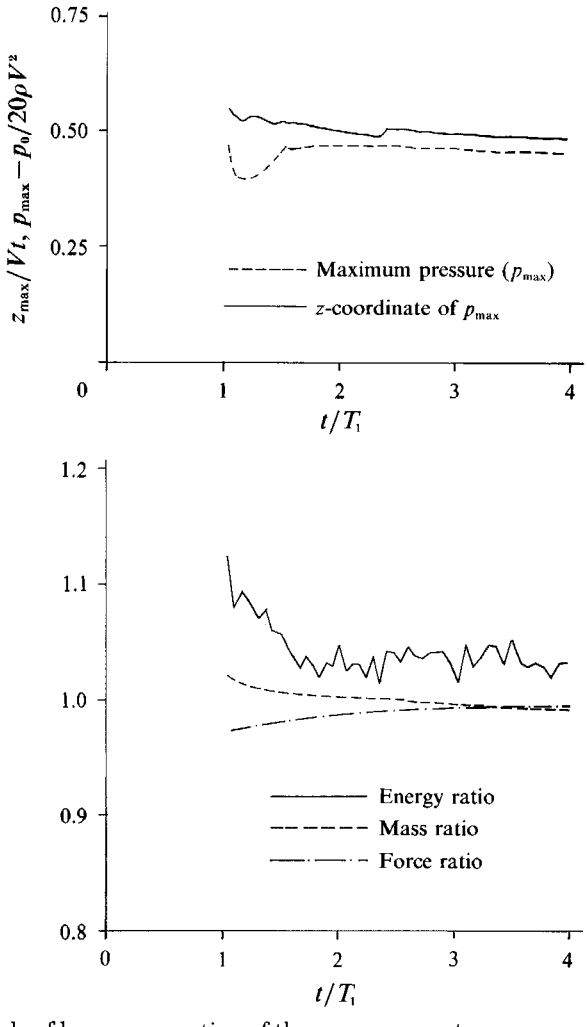

FIGURE 3. Example of how conservation of the mass, momentum, energy and similarity conditions are satisfied for a wedge that is forced with constant vertical velocity V through the free surface; $\alpha = 20°$, t = time. Calculations are based on the nonlinear boundary element method described in §2. $t = T_1$ is the time instant when the jet flow approximation is introduced.

mass above the still water level and the time derivative of the fluid mass displaced by the body below the still water level. The energy ratio is the ratio between the time derivative of (2.10) and (2.11). The time derivative of the energy is only calculated between two time instants when AB and CD are moving with the fluid velocity. In this way one can avoid including the neglected jet flow containing fast moving fluid with a lot of kinetic energy. The force ratio is the ratio between the right- and left-hand sides of (2.8). We show graphs only after the segments AB and CD are introduced at $t = T_1$. If conservation of mass, energy and momentum are satisfied, the mass, energy and force ratios should be 1. The figure shows that conservation of energy is most difficult to satisfy. The reason is that the energy expressions involve second-order derivatives while the mass and force expressions involve first-order derivatives. Second-order derivations will have less numerical accuracy than first-

order derivatives. The mean energy ratio is about 1.03 when $t/T_1 > 3$. Results in later sections will be based on $t/T_1 > 3$. The results show that $z_{\max}/(Vt)$ and $(p_{\max}-p_0)/(0.5\rho V^2)$ are nearly constant when $t/T_1 > 3$. In a similarity flow, these values should be constant as a function of time. When $t/T_1 < 1$, conservation of energy and momentum are not in general satisfactorily satisfied.

The numerical method has also been checked against the similarity solution for wedges and asymptotic formula for small deadrise angles. The similarity solution and the asymptotic formula are described in the following sections.

3. Similarity flow for wedges

Dobrovol'skaya (1969) has presented similarity solutions for flow around symmetric wedges that are forced with a constant vertical velocity V through an initially calm free surface. In the similarity flow the fluid velocity can be written as

$$\nabla\phi = VF\left(\frac{y}{Vt}, \frac{z}{Vt}\right), \tag{3.1}$$

where F is a function that Dobrovol'skaya finds by first solving the following integral equation:

$$f(t) = \frac{1}{\pi}\frac{c_0^2}{c^2}\int_0^t \frac{(1-t)^{-1-\gamma}\exp\left[t\int_0^1 \frac{f(\tau)}{\tau(\tau-t)}\mathrm{d}\tau\right]\mathrm{d}t}{\int_t^1 t^{-\frac{3}{2}}(1-t)^{-\frac{1}{2}+\gamma}\exp\left[-t\int_0^1 \frac{f(\tau)}{\tau(\tau-t)}\mathrm{d}\tau\right]\mathrm{d}t}, \tag{3.2}$$

where

$$\frac{c_0^2}{c^2} = \frac{\int_{\frac{1}{2}}^1 r^{-\frac{3}{2}}(1-r)^{-\frac{1}{2}+\gamma}(2r-1)^{-\gamma}\exp\left\{-\int_0^1 \frac{f(\tau)\,\mathrm{d}\tau}{\tau[\tau\{2-(1/r)\}-1]}\right\}\mathrm{d}r}{\int_{\frac{1}{2}}^1 (1-r)^{-1-\gamma}(2r-1)^{-1+\gamma}\exp\left\{\int_0^1 \frac{f(\tau)\,\mathrm{d}\tau}{\tau[\tau\{2-(1/r)\}-1]}\right\}\mathrm{d}r}. \tag{3.3}$$

Further $\gamma = 0.5-\alpha/\pi$. The unknown function $f(t)$ is defined for t between 0 and 1. The parameter t does not mean time in this context: $f(t)$ is bounded and is proportional to the angle of inclination of the free surface along the y-axis. $t = 1$ corresponds to the intersection point between the free surface and body surface and $t = 0$ to the point of infinity along the free surface. It can be shown that

$$f(t) = O(t^{\frac{3}{2}}) \quad \text{where} \quad t \to 0, \tag{3.4}$$

$$f(t) = F_0 - B(1-t)^{\frac{1}{2}-2\beta_0} \quad \text{when} \quad t \to 1, \tag{3.5}$$

where $\beta_0 = \beta\pi$ is the angle between the body surface and the free surface at their intersection point. F_0 and B are unknowns. Dobrovol'skaya has solved (3.2) and (3.3) by iteration for deadrise angles 30°, 60° and higher. Hughes (1972) followed a different approach and presented results for $\alpha = 45°$. The smaller the deadrise angle is, the higher the accuracy needed in the numerical computations becomes. We present a different numerical scheme capable of calculating results for deadrise angles down to 4°.

In the numerical integration of (3.2) and (3.3), the integration domain is divided into different elements. This is illustrated in figure 4 and will be described for the integration from $t = 0$ to 1. The integration from $r = \frac{1}{2}$ to 1 in (3.3) can be described in a similar way. We give an example to illustrate how the elements are chosen. The

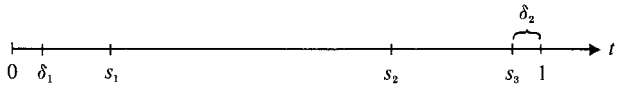

FIGURE 4. Integration domains used in the solution of Dobrovol'skaya's integral equation (3.2) for similarity flow of wedges.

reason for the distribution of elements can be understood from a detailed inspection of the integrands. From 0 to δ_1 an element length of 10^{-11} is used. From δ_1 to s_1, which is about 0.1, a linear increase in element length is used. The smallest element is next to δ_1 and is 3.63×10^{-14}. The ratio between successive elements is 1.3 and the total number of elements is 100. From s_1 to s_2, which is about 0.9, 150 elements are used. The ratio between successive elements is 1.01. The smallest element is next to s_1. From $1-\delta_2$ to 1 there is one element of length 10^{-18}. From s_2 to $s_3 = 1-\delta_2$ there are 250 elements when $\alpha \geqslant 15°$. The distribution of elements is done in two steps. The smallest one is next to $1-\delta_2$. In the first step its length is 4.49×10^{-13} and the ratio between successive elements is 1.3. In the second step the t-coordinates of the end points of the segments are chosen as

$$s_3-(1-\cos(s_3-t_i))(s_3-s_2)/(1-\cos(s_3-s_2)),$$

where t_i are the endpoints of the segments from the first step. This makes the elements closest to s_3 equal to $O(10^{-25})$. When $\alpha < 15°$, 500–1800 elements are used from s_2 to s_3.

In the integrals in (3.2) and (3.3), (3.4) is used for $t\in[0,\delta_1]$. $f(t)$ is assumed to have a linear variation over all other elements. The function

$$\exp\left[+t\int_0^1 \frac{f(\tau)}{\tau(t-\tau)}\,\mathrm{d}\tau\right]$$

in (3.2) is evaluated for t equal to the midpoints of each element. In this way the singularity at $\tau = t$ is taken properly into account. A piecewise linear variation of this function is assumed in the t-integration. The integrals over each element are calculated analytically. Equation (3.3) is handled in the same way as (3.2). The integral equation is satisfied for t-values corresponding to the endpoints of the elements.

Equation (3.2) is solved by iteration. The convergence of the iteration requires special care. In the first part of the iteration procedure, an accurate estimate of $f(1)$ is necessary. The strategy for this can be described by means of figure 5 which shows two curves with different initial guesses of $f(1)$. It is obvious that the iteration procedure diverges. The estimates have an oscillatory behaviour as a function of the number of iterations. When the oscillatory behaviour of the two curves is 180° out of phase, experience has shown that the correct value of $f(1)$ will be between the two initial guesses of $f(1)$. A better initial guess of $f(1)$ is obtained by

$$f_{01}(1)+(f_{02}(1)-f_{01}(1))[|f_{N1}(1)-f_{0\mathrm{av}}(1)|/|f_{N2}(1)-f_{N1}(1)|],$$

where $f_{Ni}(1)$ means the value of $f(1)$ after N iterations for sample number i and $f_{0\mathrm{av}} = \frac{1}{2}(f_{01}(1)+f_{02}(1))$. The typical value of N is 10. Following this procedure will finally give a solution of $f(1)$ that will oscillate with a small nearly constant amplitude for a particular value of N and then start to diverge. N may for instance be 15. The amplitude of oscillations during the first phase may be 10^{-3} relative to the mean

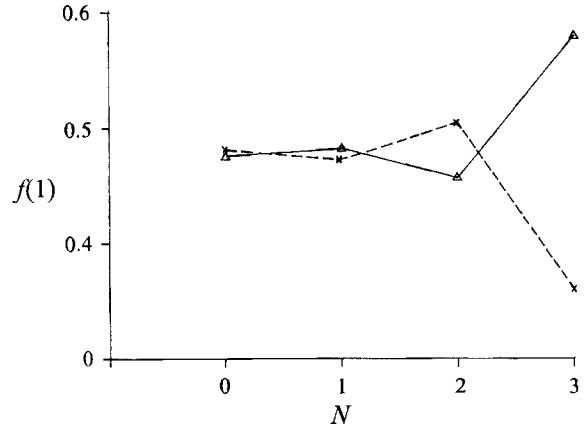

FIGURE 5. Example of the divergent behaviour of $f(1)$ as a function of the iterative solution of the integral (3.2). Two initial choices of $f(1)$ are shown. N = number of iterations.

α (deg.)	β_0/π	ζ_B/Vt	Ratio between alternative calculations		
			Mass	Energy	Force
81	0.07153	0.3872	1.0016	0.9981	0.9949
70	0.04992	0.7681	1.0018	0.9980	0.9956
60	0.03591	1.0848	1.0018	0.9976	0.9961
50	0.02514	1.3725	1.0021	0.9970	0.9962
45	0.02064	1.5038	1.0025	0.9964	0.9961
40	0.01663	1.6253	1.0029	0.9958	0.9961
30	0.009913	1.8363	1.0047	0.9935	0.9959
25	0.007143	1.9212	1.0034	0.9970	0.9986
20	0.004783	1.9955	1.0045	0.9954	0.9985
15	0.002836	2.0560	1.0057	0.9928	0.9984
10	0.001337	2.1004	1.0054	0.9923	0.9994
7.5	0.0007775	2.1174	1.0056	0.9903	0.9993
4.0	0.0002329	2.1363	1.0081	0.9749	0.9990

TABLE 1. Similarity solution results for water entry of a wedge with constant velocity V: α = deadrise angle; ζ_B = z-coordinate of the intersection point between the free surface and the body surface; β_0 = angle between the free surface and the body surface at the intersection point.

value. The other values of $f(t)$ may have a similar error relative to the mean values. To improve the solution the iterations are restarted with the values of $f(t)$ after $N-3$ iterations. The starting value of $f(1)$ is slightly changed, until the accuracy is satisfactory for all values of $f(t)$. The lower the deadrise angle is, the more difficult it is for the procedure to converge. The procedure was assumed to converge when the change in $f(t)$ between successive iterations is 10^{-8} relative to the mean value.

Table 1 shows similarity solution predictions by our numerical method for deadrise angles between 4° and 81°. The table shows ratios between alternative calculations of mass, energy and force. The ratio for the mass is the ratio between the fluid mass above the still water level and the fluid mass displaced by the body below the still water level. The ratio for the energy is the ratio between the time integral of (2.11) and (2.10). The ratio for the force is the ratio between the left- and right-hand sides

of (2.8). The table shows that ratios of mass, energy and force ratios are within 1.0 ± 0.01 except for $\alpha = 4°$. It is most difficult to satisfy conservation of energy, in particular for small deadrise angles. The table gives also predictions of the z-coordinate ζ_B of the intersection point between the free surface and the body surface, as well as the angle β_0 between the free surface and the body surface at the intersection. Dobrovol'skaya (1969) has presented values for β_0 and ζ_B for $\alpha = 30°$, 60°, 81° and higher. The results in table 1 agree with Dobrovol'skaya's results for $\alpha = 81°$, while for $\alpha = 30°$ Dobrovol'skaya predicts $\zeta_B = 2.0Vt$ and $\beta_0 = 0.011\pi$ compared to $\zeta_B = 1.84Vt$ and $\beta_0 = 0.0099\pi$ in table 1. For $\alpha = 60°$ the predictions of β_0 agree, while Dobrovol'skaya predicts $\zeta_B = 1.13Vt$. The reason for the disagreement at lower deadrise angle is believed to be that the computations require modern computer facilities with large storage capacity and rapid processing time. Hughes (1972) predicted $\beta_0 = 0.02\pi$ and $\zeta_B = 1.5Vt$ for $\alpha = 45°$. This agrees with table 1. Based on an asymptotic analysis, Cointe (1991) has proposed that $\beta_0 \pi = 0.5\alpha^2$ for small deadrise angles. The same type of asymptotic analysis will give that $\zeta_B = (\pi - 1)\,Vt$. These asymptotic results are in agreement with the results in table 1.

4. Asymptotic formula for small deadrise angles

At small deadrise angles it is possible to use matched asymptotic expansions to solve the hydrodynamic problem. It is assumed that no air pocket is created during the impact. The flow is divided into an inner and outer flow domain. In the inner flow, the details of the jet flow at the intersection between the free surface and the body are studied. The matching is shown by Armand & Cointe (1986), Cointe (1991) and Howison *et al.* (1991), and will not be repeated here. Our intention is to present a composite solution for the pressure distribution on the body, which will be used in the following section to compare with numerical results by the similarity solution and the boundary element method.

The inner flow regions are located around $y = \pm c(t)$. Here $c(t)$ is dependent on the cross-sectional form and can be found from Wagner's (1932) integral equation. For a wedge it is found that $c(t) = 0.5\pi Vt \operatorname{cotan} \alpha$. The pressure p_{out} on the body in the outer flow region can be approximated as

$$p_{out} - p_0 = \rho V c (\mathrm{d}c/\mathrm{d}t)(c^2 - y^2)^{-\frac{1}{2}} \quad \text{for} \quad |y| < c(t). \tag{4.1}$$

In the inner flow region around $y = c(t)$ the pressure p_{in} on the body surface can be found in Wagner (1932) and written as

$$p_{in} - p_0 = 2\rho[\mathrm{d}c/\mathrm{d}t]^2 |\tau|^{\frac{1}{2}} (1 + |\tau|^{\frac{1}{2}})^{-2}, \tag{4.2}$$

where $|\tau|$ is related to y by

$$y - c = (\delta/\pi)(-\ln|\tau| - 4|\tau|^{\frac{1}{2}} - |\tau| + 5). \tag{4.3}$$

The jet thickness $\delta = \pi V^2 2c[4\,\mathrm{d}c/\mathrm{d}t]^{-2}$ is obtained by matching the inner and outer solutions. The parameter $|\tau|$ varies from 0 to ∞ on the body surface. The maximum value of p_{in} occurs when $|\tau| = 1$, i.e. $y = c$. When $|\tau| \to 0, y \to \infty$ along the body on the upper side of the jet. When $|\tau| \to \infty, y \to -\infty$ along the body. For large values of $|\tau|$ we can then write $p_{in} - p_0 \sim 2\rho[\mathrm{d}c/\mathrm{d}t]^2 |\tau|^{-\frac{1}{2}}$ and $y - c \sim -(\delta/\pi)|\tau|$. This means

$$p_{in} - p_0 \sim \rho V c (\mathrm{d}c/\mathrm{d}t)[2c(c-y)]^{-\frac{1}{2}} \tag{4.4}$$

for large positive values of $c - y$.

A composite solution for the pressure distribution on the body surface for positive

y can be obtained by noting that p_{out} has the same asymptotic behaviour when $y \to c$ as (4.4). Adding p_{out} and p_{in} and subtracting the common asymptotic term given by (4.4) results in the following composite solution for $0 \leqslant y \leqslant c(t)$:

$$p - p_0 = \rho V c \frac{\mathrm{d}c}{\mathrm{d}t}(c^2 - y^2)^{-\frac{1}{2}} - \rho V c \frac{\mathrm{d}c}{\mathrm{d}t}[2c(c-y)]^{-\frac{1}{2}} + 2\rho\left(\frac{\mathrm{d}c}{\mathrm{d}t}\right)^2 |\tau|^{\frac{1}{2}}(1+|\tau|^{\frac{1}{2}})^{-2}. \quad (4.5)$$

This solution has no singular behaviour at $y = c(t)$. For $y > c(t)$ equation (4.2) is used. The pressure will be symmetric about $y = 0$.

Watanabe (1986) has also provided a solution based on matched asymptotic expansions and local jet flow analysis. However, his analysis of the jet flow, the matching and the final results are not the same as ours.

5. Comparisons of flow around wedges

Figure 6 shows numerical predictions of pressure distribution and free-surface elevation around wedges that are forced with constant vertical velocity V through an initially calm free surface. The deadrise angle is varied from 4° to 81°. All figures present results using the numerical method described in §2 and the similarity solution. The agreement between these two methods is good. The largest differences occur in the prediction of the free-surface elevation close to the jet flow and in how the pressure approaches atmospheric pressure in the jet flow. This is believed to be associated with the jet flow approximation used in the boundary element method, as discussed in §2. At small deadrise angles the pressure is sharply peaked close to the jet flow domain. Calculation of the pressure in this area requires high accuracy both for the similarity solution and the nonlinear boundary element method. A reason is that the $\rho\,\partial\phi/\partial t$-term and the velocity squared term in Bernoulli's equation are of different sign and have large and nearly equal absolute values in the jet flow area. This is illustrated in figure 7 for $\alpha = 20°$. The similarity solution has the best numerical accuracy. Table 1 shows that the ratios of mass, energy and force are within 1.0 ± 0.01 except for $\alpha = 4°$. When the nonlinear boundary element method was used, the mean energy ratios were about 1.03 for $\alpha = 40°$, 1.02 for $\alpha = 30°$, 1.03 for $\alpha = 25°$ and 20°, 1.05 for $\alpha = 15°$, 1.1 for $\alpha = 10°$, 1.06 for $\alpha = 7.5°$ and 1.08 for $\alpha = 4°$. The mean mass and force ratios were within 1.0 ± 0.01 except for $\alpha = 4°$ where the mass ratio was 0.97.

Figure 6 shows numerical similarity solution results by Dobrovol'skaya (1969) for $\alpha = 30°$ and 60° and by Hughes (1972) for $\alpha = 45°$. The agreement with our numerical similarity solution results is good for $\alpha = 45°$, while there are some differences with Dobrovol'skaya's results, in particular for $\alpha = 30°$. There must also be a misprint in Dobrovol'skaya's pressure results for $\alpha = 30°$. The results in figure 6 are believed to be correct. A reason for the disagreement may be due to a lack of accuracy in Dobrovol'skaya's numerical calculations. Dobrovol'skaya's result for $\alpha = 81°$ agree with ours.

Figure 6 also shows pressure results from the asymptotic theory for small deadrise angles (up to $\alpha = 30°$). The agreement with the similarity solution is very good for small α-values. The results for $\alpha = 4°$ shows that Watanabe's (1986) asymptotic theory differs from our asymptotic theory. Reasons why the asymptotic theory deviates for larger deadrise angles are that the quadratic velocity term in Bernoulli's equation is neglected in the outer solution, and that the body boundary condition is not satisfactorily satisfied in the outer flow solution. The velocity potential in the

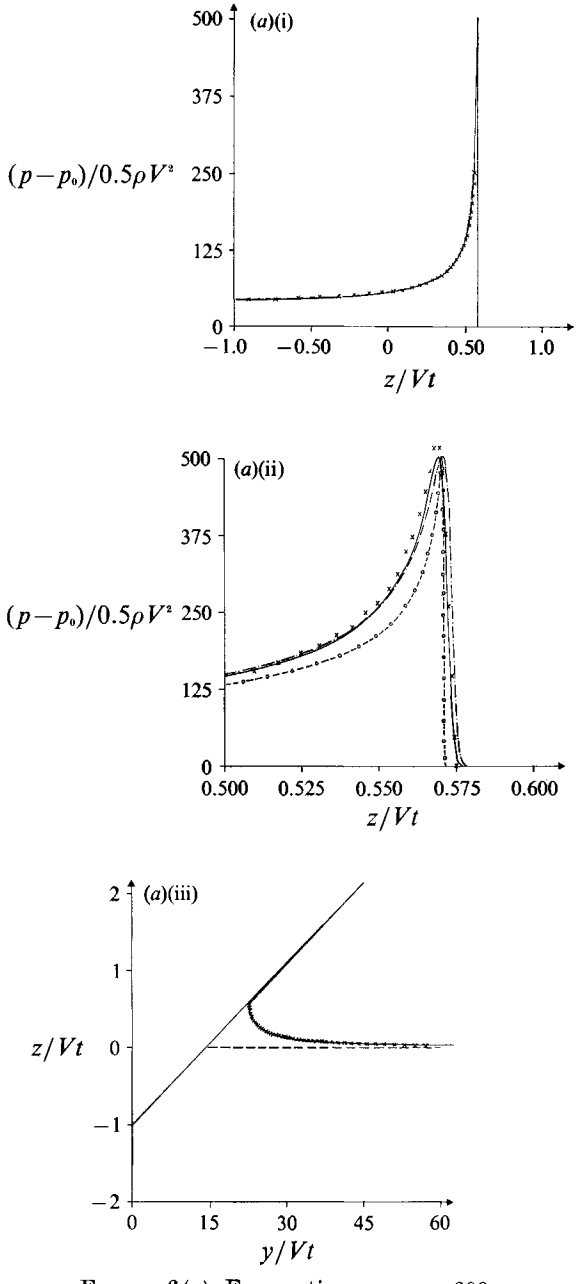

FIGURE 6(*a*). For caption see page 609.

outer solution has been obtained by transferring the body boundary condition to a straight horizontal line connecting $y = \pm c(t)$. This can only be done for small values of α. In order to match the outer flow solution to Wagner's local jet flow solution it is essential that the outer flow velocity potential is proportional to the square root of the distance from $y = \pm c(t)$ in the vicinity of $y = \pm c(t)$. For non-small values of α it is not obvious that it is possible to find an outer solution that satisfies the exact body boundary condition and matches with Wagner's solution. The reason why the

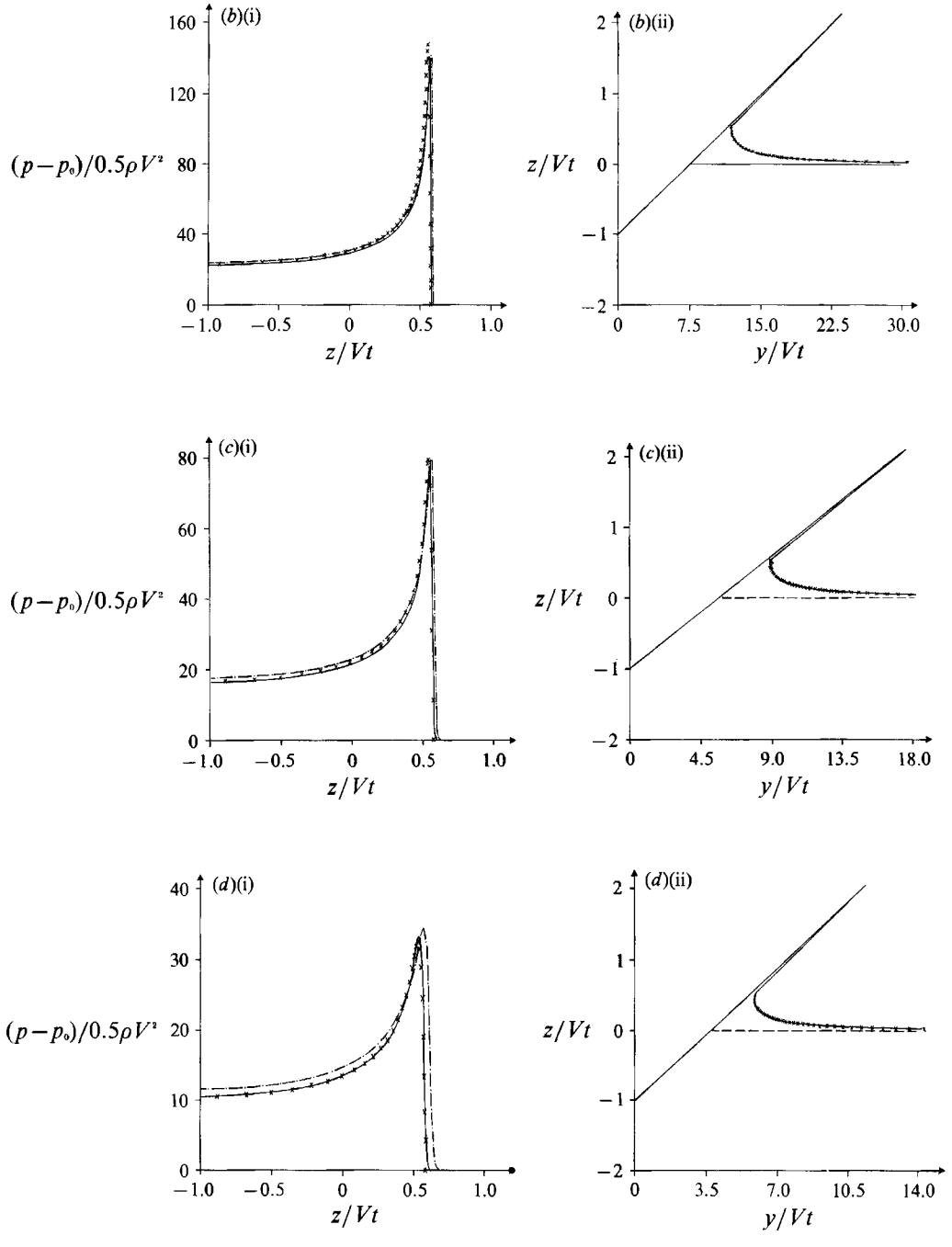

FIGURE 6(*b–d*). For caption see page 609.

asymptotic theory shows a discontinuity in the derivative at $y = c(t)$ for $\alpha = 30°$ is that there no longer exists an overlap region between the inner and outer solution.

The pressure results in figure 6 show only a typical slamming behaviour for α up to $\sim 30°$. (By slamming we mean impulse loads with high pressure occurring over a small surface area.) Important parameters characterizing slamming are the position

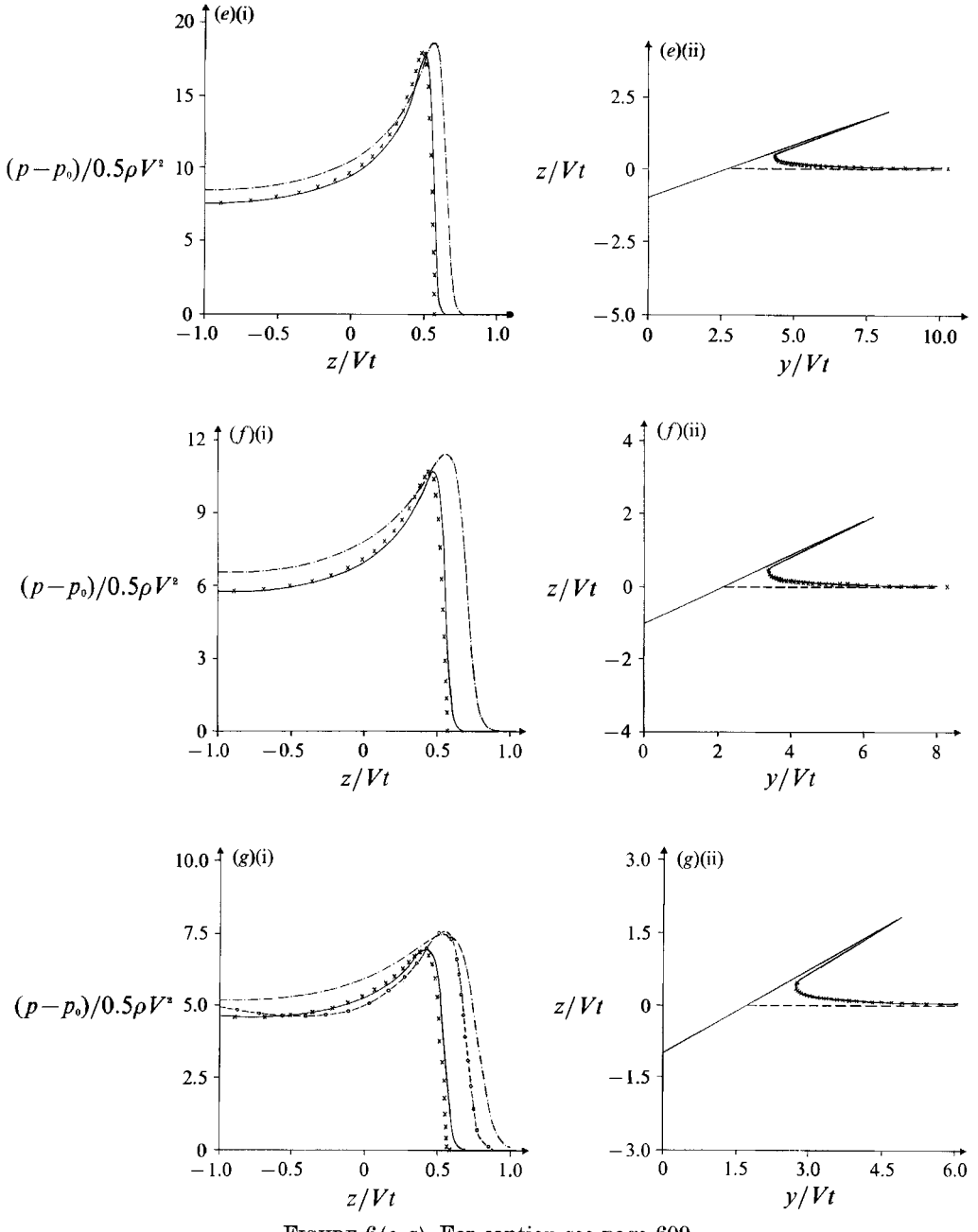

FIGURE 6(*e–g*). For caption see page 609.

and value of the maximum pressure, the time duration and the spatial extent of the slamming pressures.

According to the asymptotic theory the z-coordinate of maximum pressure is equal to $(0.5\pi-1)\,Vt$ and the maximum slamming pressure $p_{\max}$ is given by

$$C_{p_{\max}} \equiv \frac{p_{\max}-p_0}{0.5\rho V^2} = 0.25\pi^2 \operatorname{cotan}^2\alpha \tag{5.1}$$

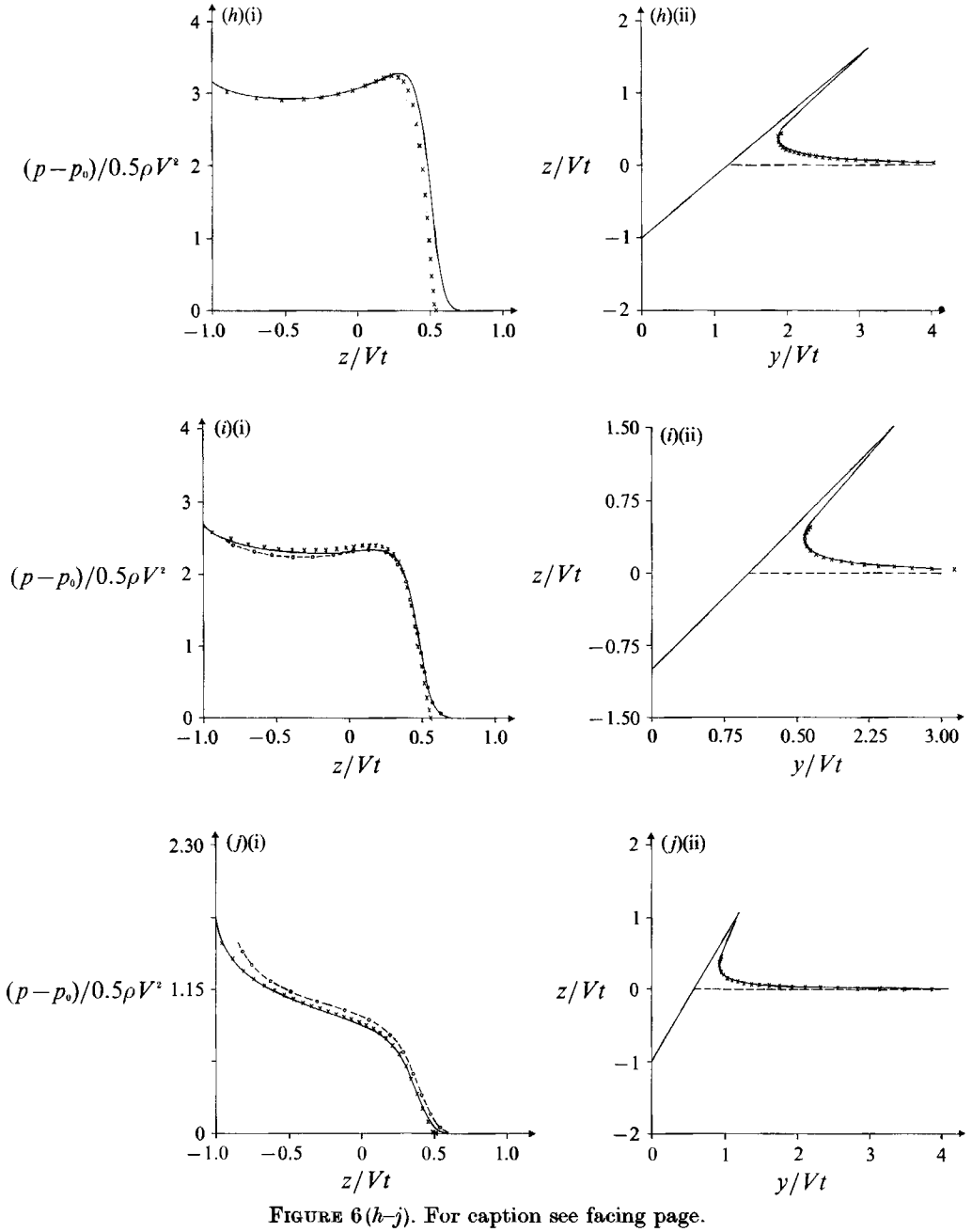

FIGURE 6(*h–j*). For caption see facing page.

for a wedge. The time duration of slamming can be quantified by considering a fixed point on the body surface and evaluating the time Δt_s it takes from when the pressure is $\frac{1}{2}(p_{\max}-p_0)$ until it is $\frac{1}{2}(p_{\max}-p_0)$ again. The spatial extent, ΔS_s, of the slamming pressure can be found in a similar way, see figure 8. Figure 6 shows that ΔS_s only has meaning when $\alpha \leqslant 20°$. Table 2 shows predictions of $C_{p_{\max}}$, $z_{\max}$, ΔS_s and the total vertical force F_3 on the wedge for deadrise angles up to 40°. F_3 is based on direct pressure integration. The values by the nonlinear boundary element method in §2

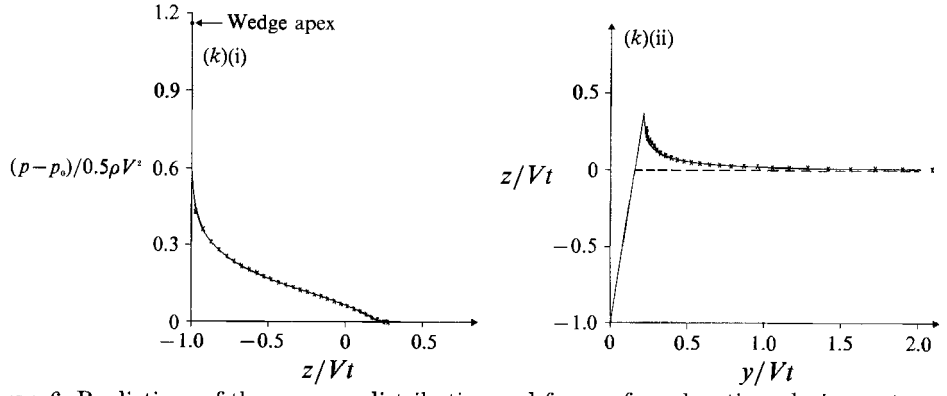

FIGURE 6. Predictions of the pressure distribution and free surface elevations during water entry of a wedge with constant vertical velocity V; α = deadrise angle: ——, similarity solution; × × × × ×, boundary element; —·—·—, asymptotic solution; —○—○—, Watanabe (1986) in (*a*) and Dobrovol'skaya (1969) in (*g*), (*j*) and Hughes (1972) in (*i*). Note the differences in the y and z scales. (*a*) $\alpha = 4°$; (*b*) 7.5°; (*c*) 10°; (*d*) 15°; (*e*) 20°; (*f*) 25°; (*g*) 30°; (*h*) 40°; (*i*) 45°; (*j*) 60°; (*k*) 81°.

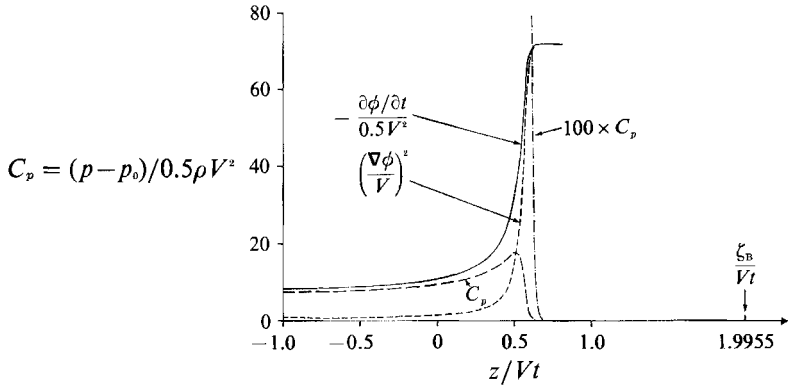

FIGURE 7. Contributions to pressure distribution from the $\rho\partial\phi/\partial t$-term and the velocity square term in Bernoulli's equation during water entry of a wedge with deadrise angle 20° and constant vertical velocity V. Calculations based on the similarity solution.

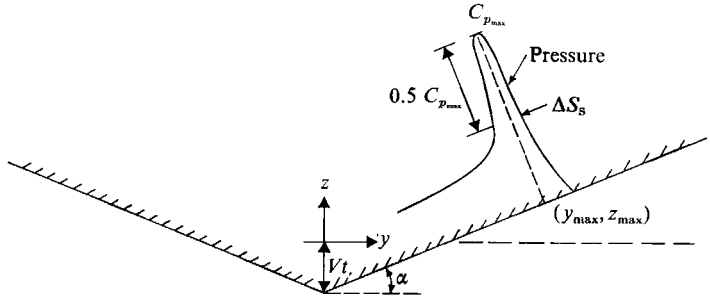

FIGURE 8. Definitions of parameters characterizing slamming pressure during water entry of a blunt two-dimensional body. C_p = pressure coefficient.

have been obtained by averaging the values in the time interval $3 < t/T_1 < t_{max}/T_1$, where t_{max}/T_1 is up to 4 and $t = T_1$ corresponds to the instant when AB and CD are introduced the first time (see figure 3 and the explanation of the figure). Table 3 gives

	$C_{p_{max}}$			z_{max}/Vt		
α (deg.)	Simil.	Asymp.	BE	Simil.	Asymp.	BE
4	503.030	504.61	521.4	0.5695	0.5708	0.571
7.5	140.587	142.36	148.3	0.5623	0.5708	0.558
10	77.847	79.36	80.2	0.5556	0.5708	0.555
15	33.271	34.37	32.8	0.5361	0.5708	0.533
20	17.774	18.63	18.2	0.5087	0.5708	0.488
25	10.691	11.35	10.9	0.4709	0.5708	0.443
30	6.927	7.40	6.94	0.4243	0.5708	0.400
40	3.266	3.50	3.26	0.2866	0.5708	0.245
	$\Delta S_s/c$			$F_3/(\rho V^3 t)$		
α (deg.)	Simil.	Asymp.	BE	Simil.	Asymp.	BE
4	0.01499	0.01576	0.0156	1503.638	1540.506	1491.8
7.5	0.05129	0.05586	0.0526	399.816	423.735	417.9
10	0.09088	0.1002	0.0941	213.980	231.973	220.8
15	0.2136	0.2314	0.226	85.522	96.879	85.5
20	0.4418	0.4270	0.434	42.485	50.639	43.0
25	—	—	—	23.657	29.765	23.7
30	—	—	—	14.139	18.747	13.9
40	—	—	—	5.477	8.322	5.31

TABLE 2. Estimation of slamming parameters by the asymptotic method, the nonlinear boundary element method (§2) and the similarity solution during water entry of a wedge with constant vertical velocity V: α = deadrise angle; $C_{p_{max}}$ = pressure coefficient at maximum pressure; z_{max} = z-coordinate of maximum pressure (see figure 8); ΔS_s = spatial extent of slamming pressure (see figure 8); $c = 0.5\pi Vt \operatorname{cotan}\alpha$; F_3 = total vertical hydrodynamic force on the wedge.

α (deg.)	σ of $C_{p_{max}}$	σ of z_{max}/Vt	σ of $\Delta S_s/c$	σ of $F_3/\rho V^3 t$
4	4.0	0.001	0.0003	20.1
7.5	1.2	0.002	0.0003	3.5
10	1.0	0.002	0.0009	1.9
15	0.3	0.002	0.002	0.5
20	0.1	0.003	0.007	0.2
25	0.1	0.004	—	0.1
30	0.05	0.011	—	0.1
40	0.01	0.004	—	0.02

TABLE 3. Standard deviations σ of slamming parameters obtained from simulation of water entry of a wedge with constant vertical velocity by means of the nonlinear boundary element method described in §2. The mean values and explanations are given in table 2.

standard deviations of the time records of the slamming parameters. The results in tables 2 and 3 show that the nonlinear boundary element method is in good agreement with the similarity solution. The asymptotic method seems to converge to the results by the similarity solution when $\alpha \to 0$. The maximum pressure is well predicted by the asymptotic method even for larger deadrise angles presented in table 2. When $\alpha \geqslant 45°$ (see figure 6), the maximum pressure is at the apex of the wedge. According to the similarity solution $C_{p_{max}}$ will be 2.720, 2.349, 1.810, 1.443 and 1.163 for respectively $\alpha = 45°$, 50°, 60°, 70° and 81°.

The results in table 2 for ΔS_s at small values of α illustrate that measurement of slamming pressure requires high sampling frequency and 'small' pressure gauges. There exist in the literature several reported experimental values for the maximum pressure for wedges and different opinions on how well Wagner's theory for the maximum pressure agrees with experimental results. However, experimental error sources due to the size of the pressure gauge and the change of the body velocity during a drop test are not always considered. Takemoto (1984) and Yamamoto, Ohtsubo & Kohno (1984) did consider these factors and showed good agreement with Wagner's theory for maximum pressure when the deadrise angle was between $\sim 3°$ and 15°. The reason for the disagreement for $\alpha < \sim 3°$ is due to the air-cushion effect under the wedge.

6. Conclusions

A numerical method for studying water entry of a two-dimensional body of arbitrary cross-section is presented. It is based on a nonlinear boundary element method. Important features are how the jet flows occurring at the intersections between the free surface and the body are handled, and how conservation of fluid mass is satisfied in areas of high curvature of the free surface. Conservation of momentum and energy are also satisfied.

The method has been verified by comparisons with similarity solutions for water entry of wedges with constant vertical velocity. The similarity solution was theoretically derived by Dobrovol'skaya (1969). In extending her results, it has been necessary to develop new numerical solutions for wedges with deadrise angles α varying from 4° to 81°.

A simple asymptotic solution for small α based on Wagner (1932) have been presented and shown to give good predictions of slamming pressures for small deadrise angles α. For α larger than approximately 30°, the pressure distribution on the body surface does not show the typical slamming behaviour of high impulse pressures concentrated over small surface areas.

The authors appreciate the comments by Dr M. Greenhow.

REFERENCES

ARMAND, J. L. & COINTE, R. 1986 Hydrodynamic impact analysis of a cylinder. In *Proc. Fifth Int Offshore Mech. and Arctic Engng Symp., Tokyo, Japan*, Vol. 1, pp. 609–634. ASME.

COINTE, R. 1991 Free surface flows close to a surface-piercing body. In *Mathematical Approaches in Hydrodynamics* (ed. T. Miloh), pp. 319–334. Soc. Ind. Appl. Maths, Philadelphia, USA.

DOBROVOL'SKAYA, Z. N. 1969 On some problems of similarity flow of fluid with a free surface. *J. Fluid Mech.* **36**, 805–829.

FALTINSEN, O. 1977 Numerical solutions of transient nonlinear free-surface motion outside or inside moving bodies. In *Proc. 2nd Intl Conf. Num. Ship. Hydrodyn., University of California, Berkeley*, pp. 347–357.

FALTINSEN, O. 1990 *Sea Loads on Ships and Offshore Structures*. Cambridge University Press.

FALTINSEN, O. & ZHAO, R. 1991 Numerical predictions of ship motions at high forward speed. *Phil. Trans. R. Soc. Lond.* A **334**, 241–252.

FRAENKEL, E. 1991 On the water entry of a wedge. *The Mathematics of Nonlinear Systems, SERC Meeting, Bath.*

GARABEDIAN, P. R. 1953 Oblique water entry of a wedge. *Commun. Pure Appl. Maths* **6**, 157–165.

GREENHOW, M. 1987 Wedge entry into initially calm water. *Appl. Ocean Res.* **9**, 214–223.

HOWISON, S. D., OCKENDON, J. R. & WILSON, S. K. 1991 Incompressible water-entry problems at small deadrise angles. *J. Fluid Mech.* **222**, 215–230.

HUGHES, O. F. 1972 Solution of the wedge entry problem by numerical conformal mapping. *J. Fluid Mech.* **56**, 173–192.

KOROBKIN, A. A. & PUKHNACHOV, V. V. 1988 Initial stage of water impact. *Ann. Rev. Fluid Mech.* **10**, 159–185.

MACKIE, A. G. 1969 The water entry problem. *Q.J. Mech. Appl. Maths* **22**, 1–17.

NEWMAN, J. N. 1977 *Marine Hydrodynamics.* The MIT Press.

TAKEMOTO, H. 1984 Some considerations on water impact pressure. *J. Soc. Naval Arch. Japan* **156**, 314–322.

VINJE, T. & BREVIG, P. 1980 Nonlinear ship motions. In *Proc. 3rd Intl Conf. Num. Ship Hydrodyn., Paris, June*, pp. 257–266.

WAGNER, H. 1932 Über stoss- und Gleitvergänge an der Oberfläche von Flüssigkeiten. *Z. Angew. Math. Mech.* **12** (4), 192–235.

WATANABE, T. 1986 Analytical expression of hydrodynamic impact pressure by matched asymptotic expansion technique. *Trans. West-Japan Soc. Naval Arch.*, No. 71, pp. 77–85.

YAMAMOTO, Y., OHTSUBO, H. & KOHNO, Y. 1984 Water impact of wedge model. *J. Soc. Naval Arch. Japan* **155**, 236–245.